Nonlinear Control of a Variable-Speed Wind Turbine Using a Two-Mass Model

Boubekeur Boukhezzar, Houria Siguerdidjane

Nonlinear Control of a Variable-Speed Wind Turbine Using a Two-Mass Model

Boubekeur Boukhezzar and Houria Siguerdidjane

***Abstract*—The paper presents a nonlinear approach, using a two-mass model and a wind speed estimator, for variable-speed wind turbine (WT) control. The use of a two-mass model is motivated by the need to deal with flexible modes induced by the low-speed shaft stiffness. The main objective of the proposed controllers is the wind power capture optimization while limiting transient loads on the drive-train components. This paper starts by an adaptation of some existing control strategies. However, their performance are weak, as the dynamics aspects of the wind and aeroturbine are not taken into consideration. In order to bring some improvements, nonlinear static and dynamic state feedback controllers, with a wind speed estimator, are then proposed. Concerning the wind speed estimator, the idea behind this is to exploit the WT dynamics by itself as a measurement device. All these methods have been first tested and validated using an aeroelastic WT simulator. A comparative study between the proposed controllers is performed. The results show better performance for the nonlinear dynamic controller with estimator in comparison with the adapted existing methods.**

***Index Terms*—Nonlinear control, power capture optimization, two-mass model, variable-speed wind turbines (VSWT).**

NOMENCLATURE

$B_{\rm ls}$	Low-speed shaft stiffness $(\mathrm{N\cdot m\cdot rad^{-1}})$.
$C_p(\lambda,\beta)$	Power coefficient.
$C_q(\lambda,\beta)$	Torque coefficient.
J_g	Generator inertia $(\mathrm{kg\cdot m^2})$.
J_r	Rotor inertia $(\mathrm{kg\cdot m^2})$.
K_g	Generator external damping $(\mathrm{N\cdot m\cdot rad^{-1}\cdot s^{-1}})$.
$K_{\rm ls}$	Low-speed shaft damping $(\mathrm{N\cdot m\cdot rad^{-1}\cdot s^{-1}})$.
K_r	Rotor external damping $(\mathrm{N\cdot m\cdot rad^{-1}\cdot s^{-1}})$.
n_g	Gearbox ratio.
P_a	Aerodynamic power (W).
P_e	Electrical power (W).
R	Rotor radius (m).
T_a	Aerodynamic torque $(\mathrm{N\cdot m})$.
$T_{\rm em}$	Generator (electromagnetic) torque $(\mathrm{N\cdot m})$.
$T_{\rm hs}$	High-speed shaft torque $(\mathrm{N\cdot m})$.
$T_{\rm ls}$	Low-speed shaft torque $(\mathrm{N\cdot m})$.
$\hat{x}$	Estimate of x.
$\dot{x},\ddot{x}$	First and second derivative of x with respect to time.
$x^{(i)}$	ith derivative of x with respect to time.
$x_{\rm opt}$	Optimal value of x.
CART	Controls advanced research turbine.
FAST	Fatigue, aerodynamics, structures, and turbulence.
VSWT	Variable-speed wind turbine.
WT	Wind turbine.
λ	Tip speed ratio.
β	Pitch angle (deg).
v	Wind speed $(\mathrm{m\cdot s^{-1}})$.
θ_g	Generator-side angular deviation (rad).
$\theta_{\rm ls}$	Gearbox-side angular deviation (rad).
θ_t	Rotor-side angular deviation (rad).
ρ	Air density $(\mathrm{kg\cdot m^{-3}})$.
ω_g	Generator speed $(\mathrm{rad\cdot s^{-1}})$.
$\omega_{\rm ls}$	Low-speed shaft speed $(\mathrm{rad\cdot s^{-1}})$
ω_t	Rotor speed $(\mathrm{rad\cdot s^{-1}})$.

The authors are with the Automatic Control Department, Supélec, Gif-sur-Yvette 91192, France.

I. INTRODUCTION

WIND power production knows since two decades a serious interest recovery. This requires the development of efficient production tools [1], [2]. The VSWTs have many advantages compared to former fixed-speed WT. The main one remains in their annual production, which exceeds by 5% to 10% fixed speed ones [3]. The effects of wind power fluctuations can also be attenuated using this kind of turbines. Moreover, it was shown that the control strategy has a major impact on the WT behavior and on the loads transmitted to the network [4], and that whatever the kind of WT, the control system remains a key factor [5].

The main objective of WT control, for low wind speeds, is to extract the maximum of power from the wind by rotating the WT rotor at a reference proportional to the effective wind speed. As matter of fact, latter is difficult to be measured. Indeed, as the wind speed varies along the rotor swept area, the measurement given by an anemometer is that of the wind speed in a single point of this area. It is, therefore, impossible to determine the mean wind speed blowing on the rotor by this measurement. Many assumptions are made in the literature to overcome this drawback. In some papers, it is assumed directly that the effective wind speed is measurable [6], [7], which amounts to assume that the WT already reaches a steady-state regime on its optimal efficiency curve [8]–[10]. Linearized models are also often used. They consider the wind speed input as a disturbance to be decoupled [11]–[13]. The high-wind speed turbulence makes this assumption untenable inducing weak performance of the associated controllers, particularly in terms of electrical efficiency. In most cases, a one-mass model of the WT is used for controller design [10], [14]–[17]. An accurate modeling of WTs is a challenging problem due to the complexity of the

mechanics and turbulent and unpredictable conditions in which they operate [18]. As commonly used for industry real-world applications, a simplified modeling is preferable (but valid in some desired operating conditions and domains) in order to elaborate a controller with not so much tuning coefficients and which demonstrates quite satisfactory results.

The contribution of this paper, with regards to the literature, is on the one hand, the consideration of a two-mass model for nonlinear controllers synthesis. Classical controllers described in the literature for a one-mass model, such as the maximum power point tracking (MPPT) [19] and the aerodynamic torque feedforward (ATF) [20] strategy were herein adapted to the two-mass model.

On the other hand, the contribution consists of proposing controllers that take into account the nonlinear nature of the WT aerodynamics, its flexible structure, using a two-mass model and the wind turbulence nature without considering that this one is measurable. The controllers use nonlinear static and dynamic state feedback, with a wind speed estimator, to track the optimal tip speed ratio. The wind speed is estimated using the WT itself as a measurement device. In doing so, the proposed controllers avoid the assumptions that the wind speed is measurable or that the WT evolves near an operating point that allows the use of a local linearized model. In addition, the synthesized controllers are able to deal with a realistic operating conditions, such as control action disturbances and measurement noise.

This paper is organized as follows. The two-mass nonlinear model is described in Section II, and then, written down in nonlinear state-space form. Section III recalls VSWT control objectives below rated power. Some existing control strategies are then adapted to the two-mass model and are also presented in this section. The wind speed estimator is described in Section IV. In Section V, two nonlinear controllers are designed: the first one uses nonlinear static state feedback and the other one nonlinear dynamic state feedback-based approaches. Both compensators are combined with the estimator and are as well tested upon the mathematical model and validated using an aeroelastic WT simulator in Section VI. Finally, a conclusion is drawn, the obtained results show better performance compared to the adapted existing methods, particularly in the presence of measurement noise and input disturbance.

II. WT MODELING

The aerodynamic power captured by the rotor is as follows:

$$P_a = \frac{1}{2}\rho\pi R^2 C_p(\lambda,\beta)v^3. \tag{1}$$

The power coefficient C_p depends on both the blade pitch angle β and the tip speed ratio λ, which is defined as follows:

$$\lambda = \frac{\omega_t R}{v} \tag{2}$$

where ω_t is the rotor speed, R is the rotor radius, and ρ is the air density.

The aerodynamic power can then be expressed as follows:

$$P_a = \omega_t T_a. \tag{3}$$

The aerodynamic torque T_a is also given by

$$T_a = \frac{1}{2}\rho\pi R^3 C_q(\lambda,\beta)v^2 \tag{4}$$

where

$$C_q(\lambda,\beta) = \frac{C_p(\lambda,\beta)}{\lambda} \tag{5}$$

is the torque coefficient.

The power coefficient curve $C_p(\lambda,\beta)$ of the WT considered in this paper is shown in Fig. 1(a). It is obtained using the blade element theory, evaluated by a code developed by NREL,[1] and implemented using a look-up table.

The rotor inertia J_r is driven at a speed ω_t by the aerodynamic torque T_a. Its dynamics are described by

$$J_r\dot{\omega}_t = T_a - T_{\rm ls} - K_r\omega_t. \tag{6}$$

The low-speed shaft torque $T_{\rm ls}$ acts as a breaking torque on the rotor. Indeed, it results from the stiffness and damping efforts due to the difference between ω_t and $\omega_{\rm ls}$

$$T_{\rm ls} = K_{\rm ls}(\theta_t - \theta_{\rm ls}) + B_{\rm ls}(\omega_t - \omega_{\rm ls}) \tag{7}$$

The generator inertia J_g is driven by the high-speed shaft torque $T_{\rm hs}$ and braked by the electromagnetic torque $T_{\rm em}$ that it develops, so that

$$J_g\dot{\omega}_g = T_{\rm hs} - K_g\omega_g - T_{\rm em}. \tag{8}$$

The torque and the speed of this shaft are transmitted via the gearbox with a rate ratio n_g. For an ideal gearbox, one has

$$n_g = \frac{T_{\rm ls}}{T_{\rm hs}} = \frac{\omega_g}{\omega_{\rm ls}} = \frac{\theta_g}{\theta_{\rm ls}}. \tag{9}$$

Using (6)–(9), the following system is then derived:

$$\begin{bmatrix}\dot{\omega}_t\\ \dot{\omega}_g\\ \dot{T}_{\rm ls}\end{bmatrix} = \begin{bmatrix}a_{11} & a_{12} & a_{13}\\ a_{21} & a_{22} & a_{23}\\ a_{31} & a_{32} & a_{33}\end{bmatrix}\begin{bmatrix}\omega_t\\ \omega_g\\ T_{\rm ls}\end{bmatrix} + \begin{bmatrix}b_{11}\\ b_{21}\\ b_{31}\end{bmatrix}T_a + \begin{bmatrix}b_{12}\\ b_{22}\\ b_{32}\end{bmatrix}T_{\rm em} \tag{10}$$

with

$$a_{11} = -\frac{K_r}{J_r} \quad a_{12} = 0 \quad a_{13} = -\frac{1}{J_r}$$

$$a_{21} = 0 \quad a_{22} = -\frac{K_g}{J_g} \quad a_{23} = \frac{1}{n_g J_g}$$

$$a_{31} = \left(K_{\rm ls} - \frac{B_{\rm ls}K_r}{J_r}\right)$$

$$a_{32} = \frac{1}{n_g}\left(\frac{B_{\rm ls}K_r}{J_g} - K_{\rm ls}\right)$$

$$a_{33} = -B_{\rm ls}\left(\frac{J_r + n_g^2 J_g}{n_g^2 J_g J_r}\right)$$

and

$$b_{11} = \frac{1}{J_r} \quad b_{12} = 0$$

[1] National Renewable Energy Laboratory (NREL), Golden, CO.

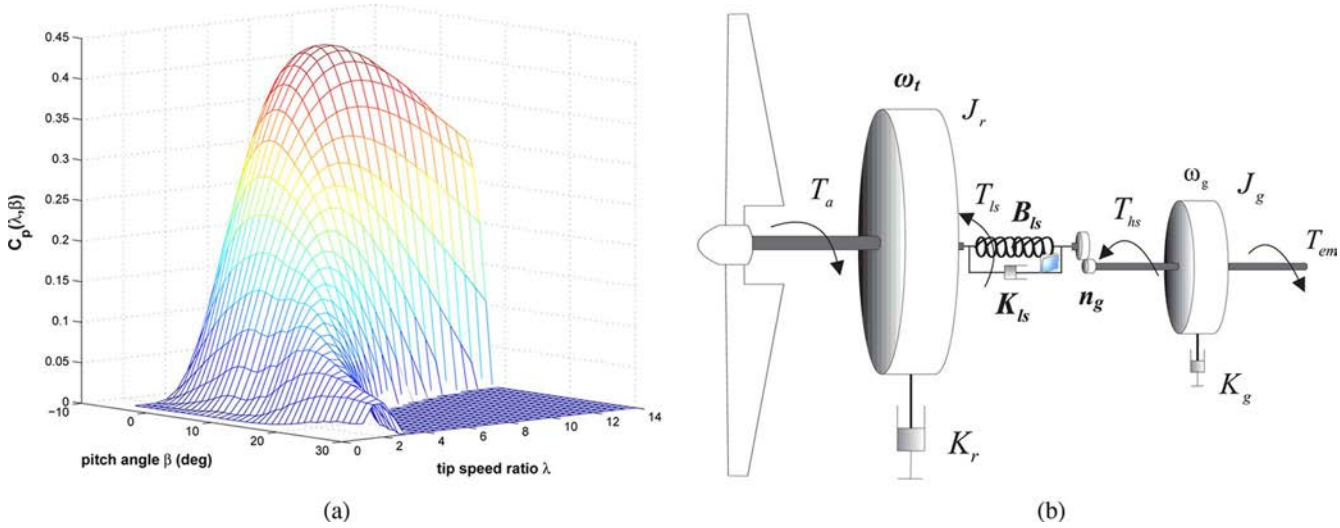

Fig. 1. WT mechanical and aerodynamical characteristics. (a) Power coefficient $C_P(\lambda, \beta)$ curve. (b) Two-mass model of the aeroturbine.

$$b_{21} = 0 \quad b_{22} = -\frac{1}{J_g}$$

$$b_{31} = \frac{B_{\rm ls}}{J_r} \quad b_{22} = \frac{B_{\rm ls}}{n_g J_g}.$$

The mechanical WT model complexity depends on its previewed use. As short as the simulation time, as the consideration of highest frequency phenomena is needed. More mass and degrees of freedom (DOFs) are then considered for modeling. In the literature, one may found the models that assume flexibility in both low- and high-speed shafts [21]. There are also more complex models that consider the mechanical model of the aeroturbine as the junction of many rigid bodies across flexible links [22], [23]. In [24], the transient stability of power systems including a VSWT generators system is analyzed using a six-mass, three-mass, and two-mass drive-train models. It has been shown that the six-mass model can be transformed to a two-mass model. The study concluded that two-mass shaft model is sufficient, with reasonable accuracy, for the transient stability analysis of wind turbine generation systems (WTGS). Three different drive-train mass models, respectively, one-, two-, and three-mass models, and three different topologies for the power electronic converters are considered in [25] to study the harmonic assessment with a fractional-order control strategy. The results have shown that the three-mass model may be more appropriate for the precise harmonic assessment of VSWTs. The objective of transient harmonic behavior reduction during a start-up operation motivates the use of a three-mass model as the simulation time is short (few seconds). In [26], the dynamic performance of fixed and variable WTs is assessed for various representations of the rotor structural dynamics, during a fault. A three-mass model that takes into account both shaft and blade flexibilities is first developed. The representation of both shaft and blade flexibilities increases the order of model. Therefore, the three-mass model was reduced to an effective two-mass model. From the previous discussion, it can be concluded that a multimass model of the structural dynamics of the WT rotor can be reduced to an effective two-mass model with an acceptable accuracy, and also that more than two-mass model may be more appropriate for short-time phenomena as transient stability analysis during faults. The choice of the adopted two-mass model with a flexible low-speed shaft is motivated by the following reasons.

1) The low-speed shaft encounters a torque n_g times greater than the high-speed shaft torque that turns n_g times more quickly than the low-speed shaft. As the low-speed shaft encounters a higher torque, it is subject to more deviation and it is more convenient to take it into consideration.
2) The use of two flexible shafts leads to a more complex model not really well adapted for controllers design.
3) Many authors report that the general models can be largely simplified to be used in control design [22]–[24].
4) The work presented here is concerned with power capture optimization during a time interval, where the mean wind speed is considered as constant (10 min). Therefore, the use of a two-mass model is largely sufficient.

Furthermore, the shaft deviation between its two sides produces the shaft torque, thus creating an internal equilibrium as the torque is constant along all the same shaft. As shown in (7), the low-speed shaft torque is proportional to the difference between ω_t and $\omega_{\rm ls}$ and between θ_t and $\theta_{\rm ls}$. The proposed control laws elaborated from this model are more general and can be applied for all-sizes WTs. Particularly, these control laws are more adapted for high-flexibility WTs, which cannot be properly modeled with a one-mass model [27], [28]. The two-mass model used in this paper assumes a flexible low-speed shaft and a rigid high-speed shaft. It has been validated by using the simulator FAST developed by NREL.

III. Problem Formulation

A. Controller Objectives

One can mainly distinguish two operating areas of a VSWT: below and above the rated power (i.e., rated wind speed).

Below the rated power, the main control objectives are as follows.

1) Wind power capture maximization.
2) Transient low-speed shaft loads minimization.

The power capture $C_p(\lambda, \beta)$ curve has a unique maximum that corresponds to an optimal capture of the wind power (see Fig. 1 (a))

$$C_p(\lambda_{\rm opt}, \beta_{\rm opt}) = C_{p_{\rm opt}} \tag{11}$$

where

$$\lambda_{\rm opt} = \frac{\omega_{t_{\rm opt}} R}{v}. \tag{12}$$

Consequently, for a partial load operating regime, and in order to maximize the wind power capture, the blade pitch angle β is fixed to its optimal value $\beta_{\rm opt}$ and in order to maintain λ at its optimal value, the rotor speed must be adjusted to track the optimal reference $\omega_{t_{\rm opt}}$ given by

$$\omega_{t_{\rm opt}} = \frac{\lambda_{\rm opt}}{R} v. \tag{13}$$

One may obviously observe that this reference has the same shape as the wind speed.

The aim of the controller is to track this optimal rotor speed $\omega_{t_{\rm opt}}$, while trying to reduce the control stress and dynamic loads.

The WT electric system time responses are much faster than those of the other components of the WT. This makes it possible to dissociate the generator and the aeroturbine control (mechanical and aerodynamic parts) designs, and thus, define a cascaded control structure through two control loops.

1) The inner control loop concerns the electric generator via the power converters.
2) The outer control loop concerns the aeroturbine that provides the reference input of the inner loop.

For WTs equipped with a doubly fed induction generator (DFIG), a back-to-back converter is used. It allows power at arbitrary frequencies to be supplied to the system at the system frequency and enables the WT to operate at variable speed [29]. Many other research works address the electrical part control without considering the aeroturbine control as, for instance, in [30]. Making the assumption that the internal (electrical) loop is well controlled, this paper focuses on the aeroturbine control. The electric generator control is not considered, since the aim of the paper is to design high-level controllers considering the rotor torque as control input. The control of both generator and aeroturbine using a one-mass model have been studied in previous work [31], [32]. In this paper, the proposed controllers deal with power capture optimization only. Above the rated wind speed, we have proposed a multivariable controllers, where a nonlinear torque controller cooperates with a proportional-integral (PI) pitch one [28].

B. Adapted Classical Controllers

In order to compare the proposed approaches with the existing controllers, two commonly encountered controllers are adapted to the two-mass model (Fig. 2). They will be briefly presented.

1) ATF Controller: In [20], an ATF controller is employed. This controller is adapted to the two-mass model. The extended state $\boldsymbol{x} = [\,\hat{\omega}_t \quad \hat{\omega}_g \quad \hat{T}_{\rm ls} \quad \hat{T}_a\,]^T$ is then estimated using a Kalman filter. The estimated aerodynamic torque is fed back in the generator reference torque. A proportional action is then used, leading to the following control expression:

$$T_{\rm em} = \frac{1}{n_g}\hat{T}_a - \left(\frac{K_r}{n_g^2} + K_g\right)\hat{\omega}_g - \frac{K_c}{n_g^2}\left(\omega_{g_{\rm ref}} - \hat{\omega}_g\right) \tag{14}$$

with

$$\omega_{g_{\rm ref}} = n_g k_\omega \sqrt{\hat{T}_a} \qquad k_\omega = \frac{1}{\sqrt{k_{\rm opt}}} = \sqrt{\frac{2\lambda_{\rm opt}^3}{\rho\pi R^5 C_{p_{\rm opt}}}}$$

and

$$k_{\rm opt} = \frac{1}{2}\rho\pi\frac{R^5}{\lambda_{\rm opt}^3} C_{p_{\rm opt}}. \tag{15}$$

However, this control strategy does not obviously cancel the steady-state error. As a drawback, it considers the WT in an optimal regime with an optimal rotational speed. The wind speed is then assumed to be constant, but unfortunately, the high-wind speed turbulence makes this assumption untenable.

2) Maximum Power Point Tracking: In [19], it was shown that a WT is stable around its optimal aerodynamic efficiency curve. It is, therefore, possible to maintain T_a on this curve by an appropriate choice of $T_{\rm em}$. For the two-mass WT model, the value of the electromagnetic torque is given by

$$T_{\rm em} = k_{{\rm opt}_{\rm hs}}\omega_g^2 - K_{t_{\rm hs}}\omega_g \tag{16}$$

where

$$k_{{\rm opt}_{\rm hs}} = \frac{k_{\rm opt}}{n_g^3} = \frac{1}{2}\rho\pi\frac{R^5}{n_g^3\lambda_{\rm opt}^3} C_{p_{\rm opt}} \tag{17}$$

and

$$K_{t_{\rm hs}} = \left(K_g + \frac{K_r}{n_g^2}\right).$$

$K_{t_{\rm hs}}$ is the low-speed shaft damping coefficient brought up to the high-speed shaft (generator).

This strategy is known in the literature as the MPPT. Considering these two methods, the transitions caused by high wind speed variations are followed by significant power losses. In summary, they present two main drawbacks: on the one hand, they do not take into consideration the dynamic aspect of the wind and the WT.

Consequently, in order to overcome the aforementioned drawbacks, a nonlinear state feedback controller based on the two-mass model is herein applied. It uses a wind speed estimator that allows to take into consideration the turbulent nature of the wind. This control structure also allows the rejection of input disturbances, acting on the electromagnetic torque $T_{\rm em}$.

IV. Wind Speed Estimation

The wind speed v involved in the aerodynamic equations is an effective value that cannot be directly measured. As this one is crucial to deduce the optimal rotor speed $\omega_{t_{\rm opt}}$, a wind speed estimator is developed using the WT itself as a measurement device. As indicated in Fig. 3, the estimator is composed of two blocks.

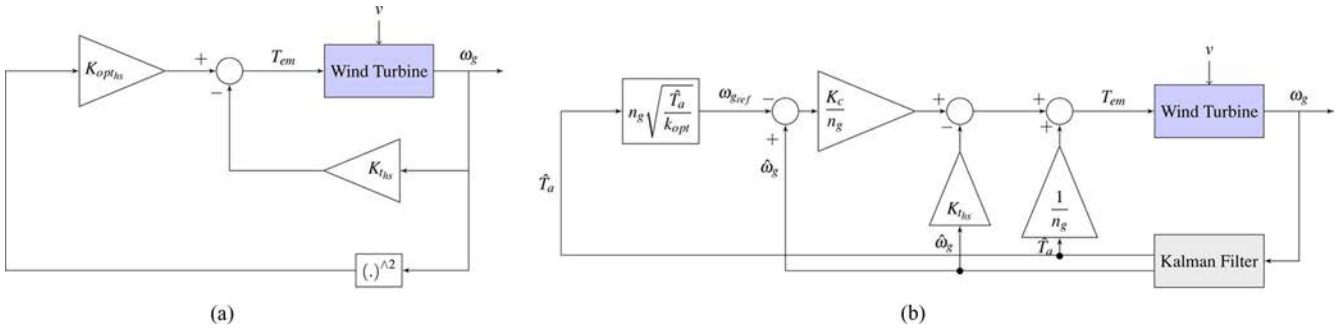

Fig. 2. Adapted classical two-mass controllers. (a) Two-mass MPPT controller curve. (b) Two-mass ATF controller.

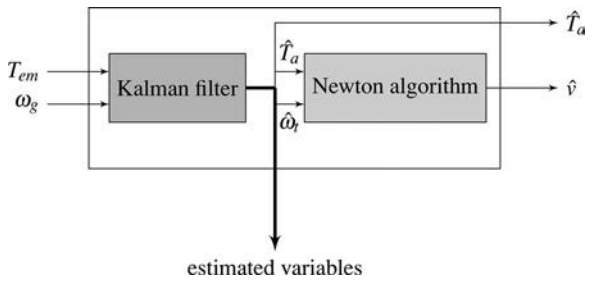

Fig. 3. Aerodynamic torque and wind speed estimator.

1) A first block, that allows to estimate, from the generator speed measurement ω_g and the electromagnetic control torque $T_{\rm em}$, the value of the aerodynamic torque $\hat{T}_a$, of the rotor speed $\hat{\omega}_t$ and the generator speed $\hat{\omega}_g$.
2) A second block with, as input, the estimates $\hat{T}_a$ and $\hat{\omega}_t$ of the aerodynamic torque and the rotor speed, respectively. The block output is the effective wind speed estimate $\hat{v}$.

The estimation of v goes through T_a one, whose estimate as well as those of the other state variables are obtained using Kalman filter (see Fig. 4).

A. Aerodynamic Torque Estimation

With the aerodynamic torque as an additional state, the augmented state-space representation is then given by (18) and (19), ξ is the process noise, and ν is the measurement noise.

Only the generator speed, which is a noisy measurement, is assumed to be available. Generally, the state and measurement noise are assumed to be stationary, the Kalman gain matrix can then be calculated offline. The Kalman filter considered in this paper is invariant even if the variance of the aerodynamic torque changes over time.

B. Wind Speed Computation

The estimate of the wind speed $\hat{v}$ is related to the one of $\hat{T}_a$ by the following equation:

$$\hat{T}_a - \frac{1}{2}\rho\pi R^3 C_q\left(\frac{\hat{\omega}_t R}{\hat{v}}\right)\hat{v}^2 = 0 \tag{20}$$

where $C_q(\hat{\lambda}) = C_q(\hat{\lambda}, \beta_{\rm opt})$ is a tabulated function of $\hat{\lambda}$. In order to use a numerical method for (20) solved with respect to $\hat{v}$, this function is interpolated with a polynomial in λ

$$C_q(\lambda) = \sum_{i=0}^{n} \alpha_i \lambda^i. \tag{21}$$

The Newton–Raphson algorithm, detailed in Appendix A, is then used to calculate $\hat{v}$. This value is exploited to deduce the optimal rotor speed $\hat{\omega}_{t_{\rm opt}} = \lambda_{\rm opt}\hat{v}/R$.

V. Nonlinear Control With Estimator

A. Nonlinear Control With Static State Feedback

From

$$\dot{\omega}_t = \frac{1}{J_r}T_a - \frac{K_r}{J_r}\omega_t - \frac{1}{J_r}T_{\rm ls}. \tag{22}$$

$$\begin{bmatrix}\dot{\omega}_t\\ \dot{\omega}_g\\ \dot{T}_{\rm ls}\\ \dot{T}_a\end{bmatrix} = \begin{bmatrix} -\frac{K_r}{J_r} & 0 & -\frac{1}{J_r} & \frac{1}{J_r}\\ 0 & -\frac{K_g}{J_g} & \frac{1}{n_g J_g} & 0\\ \left(K_{\rm ls} - \frac{B_{\rm ls}K_r}{J_r}\right) & \frac{1}{n_g}\left(\frac{B_{\rm ls}K_g}{J_g} - K_{\rm ls}\right) & -B_{\rm ls}\left(\frac{J_r + n_g^2 J_g}{n_g^2 J_g J_r}\right) & \frac{B_{\rm ls}}{J_r}\\ 0 & 0 & 0 & 0\end{bmatrix}\begin{bmatrix}\omega_t\\ \omega_g\\ T_{\rm ls}\\ T_a\end{bmatrix} + \begin{bmatrix}0\\ -\frac{1}{J_g}\\ \frac{B_{\rm ls}}{n_g J_g}\\ 0\end{bmatrix} T_{\rm em} + \begin{bmatrix}0\\0\\0\\ \xi\end{bmatrix} \tag{18}$$

$$y = \begin{bmatrix}0 & 1 & 0 & 0\end{bmatrix}\begin{bmatrix}\omega_t\\ \omega_g\\ T_{\rm ls}\\ T_a\end{bmatrix} + \nu \tag{19}$$

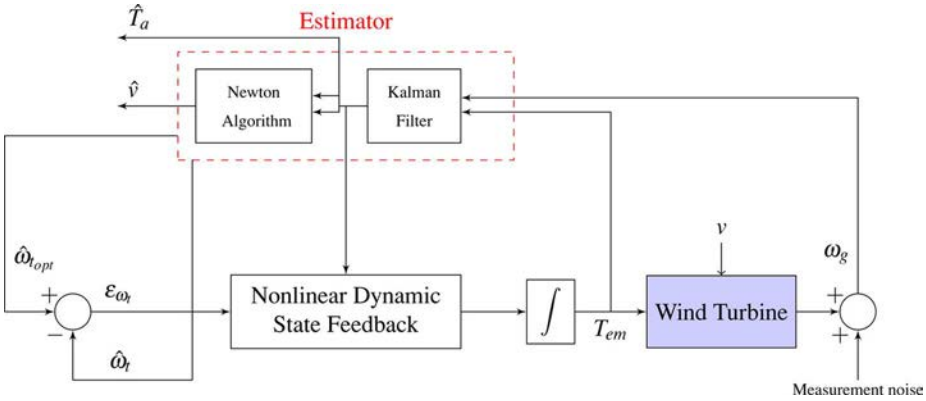

Fig. 4. Two-mass NDSFE controller.

One can deduce the expression of the second-time derivative of the rotor speed as follows:

$$\ddot{\omega}_t = \frac{1}{J_r}\dot{T}_a - \frac{K_r}{J_r}\dot{\omega}_t - \frac{1}{J_r}\dot{T}_{\rm ls}. \tag{23}$$

It is, hence, possible to extract $\dot{T}_{\rm ls}$ from (10)

$$\dot{T}_{\rm ls} = a_{31}\omega_t + a_{32}\omega_g + a_{33}T_{\rm ls} + b_{31}T_a + b_{32}T_{\rm em}. \tag{24}$$

By replacing (22) and (24) in (23), it yields

$$\ddot{\omega}_t = \frac{\dot{T}_a}{J_r} - \frac{(K_r + b_{31}J_r)}{J_r^2}T_a + \frac{(K_r^2 - a_{31}J_r)}{J_r^2}\omega_t - \frac{a_{32}}{J_r}\omega_g + \frac{(K_r - a_{33}J_r)}{J_r^2}T_{\rm ls} - \frac{b_{32}}{J_r}T_{\rm em}. \tag{25}$$

Now, let ε_ω be the tracking error defined as follows:

$$\varepsilon_\omega = \omega_{t_{\rm opt}} - \omega_t \tag{26}$$

for which one imposes second-order dynamics

$$\ddot{\varepsilon}_\omega + b_1\dot{\varepsilon}_\omega + b_0\varepsilon_\omega = 0 \tag{27}$$

b_0 and b_1 are chosen such that the polynomial $s^2 + b_1 s + b_0$ is Hurwitz.

Substituting $\dot{\omega}_t$ given by (22), and $\ddot{\omega}_t$ given by (25), and by replacing all the state variables by their estimates, it comes out the expression of the control action

$$T_{\rm em} = A_1\hat{\omega}_t + A_2\hat{\omega}_g + A_3\hat{\dot{T}}_{\rm ls} + A_4\hat{\dot{T}}_a + A_5\hat{\ddot{T}}_a + A_6(\hat{\dddot{\omega}}_{t_{\rm opt}} + b_1\hat{\ddot{\omega}}_{t_{\rm opt}} + b_0\hat{\dot{\omega}}_{t_{\rm opt}}) \tag{28}$$

with

$$A_1 = \frac{(b_0J_r^2 - b_1K_rJ_r - a_{31}J_r + K_r^2)}{b_{32}J_r} \quad A_2 = \frac{-a_{32}}{b_{32}}$$

$$A_3 = \frac{(K_r - b_1J_r - a_{33}J_r)}{b_{32}J_r} \quad A_4 = \frac{(b_1J_r - b_{31}J_r - K_r)}{b_{32}J_r}$$

$$A_5 = \frac{1}{b_{32}} \quad A_6 = \frac{-J_r}{b_{32}}.$$

The time derivative is approximated by a filtered derivative $s/1+as$, which obviously acts as a low-pass filter. As commonly used, a must be quite small (at least 10 times less than the derivative time constant). However, for the filtered derivative with a quite small a, the simulations time is too much long and the input signal disturbance is badly filtered. It turns out that the value $a = 10$ seems to achieves a good compromise.

B. Nonlinear Control With Dynamic State Feedback

In order to reject the effect of a constant additive disturbance on the control action, third-order dynamics are now imposed to the tracking error

$$\overset{(3)}{\varepsilon}_\omega + b_2\ddot{\varepsilon}_\omega + b_1\dot{\varepsilon}_\omega + b_0\varepsilon\omega = 0. \tag{29}$$

Similarly, b_0, b_1, and b_2 are chosen such that the polynomial $s^3 + b_2s^2 + b_1s + b_0$ is Hurwitz.

Starting from expression (25) of $\ddot{\omega}_t$, calculating its time derivative, and taking into consideration relationship (22) for $\dot{\omega}_t$ and (24) for $\dot{T}_{\rm ls}$, one gets the expression as following:

$$\overset{(3)}{\omega}_t = B_1\omega_t + B_2\omega_g + B_3T_{\rm ls} + B_4T_a + B_5\dot{T}_a + B_6\ddot{T}_a + B_7T_{\rm em} + B_8\dot{T}_{\rm em} \tag{30}$$

with

$$B_1 = \frac{\left[a_{31}J_r(K_r - a_{33}J_r) - K_r(K_r^2 - a_{31}J_r)\right]}{J_r^3}$$

$$B_2 = \frac{a_{32}\left[K_gJ_r + J_g(K_r - a_{33}J_r)\right]}{J_r^2J_g}$$

$$B_3 = \frac{\left[n_gJ_gJ_ra_{33}(K_r - a_{33}J_r) - a_{32}J_r^2 - n_gJ_g(K_r^2 - a_{31}J_r)\right]}{n_gJ_gJ_r^3}$$

$$B_4 = \frac{\left[b_{31}J_r(K_r - a_{33}J_r) + (K_r^2 - a_{31}J_r)\right]}{J_r^3}$$

$$B_5 = -\frac{(K_r + b_{31}J_r)}{J_r^2} \quad B_6 = \frac{1}{J_r}$$

$$B_7 = \frac{b_{32}J_g(K_r - a_{33}J_r) + a_{32}J_r}{J_r^2J_g} \quad B_8 = -\frac{b_{32}}{J_r}$$

and by substituting this expression in (29), and also $\dot{\omega}_t$ and $\ddot{\omega}_t$ given by (22) and (25), respectively, the control dynamics are thus

$$\dot{T}_{\rm em} = C_1\dddot{\hat{T}}_a + C_2\ddot{\hat{T}}_a + C_3\dot{\hat{T}}_a + C_4\dot{\hat{\omega}}_t + C_5\hat{\omega}_g + C_6\hat{T}_{\rm ls} + C_7 T_{\rm em} + C_8(\dddot{\hat{\omega}}_{t_{\rm opt}} + b_2\ddot{\hat{\omega}}_{t_{\rm opt}} + b_0\dot{\hat{\omega}}_{t_{\rm opt}}). \quad (31)$$

The coefficients C_i are hereafter given by (32). as shown at the bottom of this page.

Moreover, in order to make a compromise between power capture optimization and transient loads reduction, the following measures were adopted.

1) The choice of dynamics that track the mean tendency wind speed, along a short time interval, while avoiding to track the wind speed local high-turbulence fluctuations.
2) Filtering the aerodynamic torque $T_{\rm em}$ using a low-pass filter in order to smooth the control action. In this way, the drive train is relieved from strong loads caused by fast control torque variations.
3) Filtering the reference speed $\omega_{t_{\rm opt}}$ and its time derivatives to obtain a less turbulent signal, as shown in (32) at the bottom of the page.

The nonlinear dynamic state feedback with estimator (NDSFE) controller is designed to counter a constant additive control input disturbance (Fig. 4). The nonlinear static state feedback with estimator (NSSFE) controller imposes a second-order dynamics to the tracking error ε_ω, while the NDSFE imposes a third-order dynamics to this error. In Section VI, it is shown that with the same time response, the NDSFE controller develops less control torque than the NSSFE and encounters less deviation from the optimal rotor speed reference. One has to distinguish between the MPPT and ATF controllers from one side, and the dynamics NDSFE and NSSFE controllers from other side. The first use a static model for controllers design and assumes the WT in a steady-state regime or near the optimal behavior curve, while the second uses the two-mass dynamic model and consider the WT at any operating point with a high turbulence wind speed profile. In opposition to the NSSFE and NDSFE controllers, the dynamics of the MPPT controller are imposed by the turbine characteristics as $k_{\rm opt_{hs}}$ and $K_{t_{\rm hs}}$ in (16) depends only on the WT parameters. No DOF is allowed for MPTT controller design. The ATF controller has a single tuning parameter K_c that only allows to reduce the steady-state error. The NSSFE and NDSFE controllers allow completely the choice of the closed-loop dynamics via the tuning parameters A_i for the NSSFE and C_i for the NDSFE.

VI. Validation Results

The numerical simulations are performed with the parameters of CART WT built in NREL site nearby Colorado. CART is a bipales variable speed, variable-pitch WT. The CART generator is a squirrel-cage induction generator directly connected to the gearbox. It is connected to the grid through full-processing power electronics that can directly control generator torque [33]. The power electronics consists of a back-to-back pulsewidth modulation (PWM) converter. It is composed of two three-phase PWM converters with a common dc-link voltage. It allows a variable-speed operation by decoupling the turbine rotor speed

$$C_1 = \frac{1}{b_{32}}$$

$$C_2 = -\frac{(K_r + (b_{31} - b_2)J_r)}{b_{32}J_r}$$

$$C_3 = -\frac{\left[b_2 J_r(K_r + b_{31}J_r) - b_1 J_r^2 - b_{31}J_r(K_r - a_{33}J_r) - K_r^2 + a_{31}J_r\right]}{b_{32}J_r^2}$$

$$C_4 = -\frac{\left[K_r(K_r^2 - a_{31}J_r) - b_2 J_r(K_r^2 - J_r a_{31}) + b_1 K_r J_r^2 - b_0 J_r^3 - a_{31}J_r(K_r - a_{33}J_r)\right]}{b_{32}J_r^2}$$

$$C_5 = -\frac{a_{32}\left[J_r J_g - K_g J_r - J_g(K_r - a_{33}J_r)\right]}{b_{32}J_r J_g}$$

$$C_6 = -\frac{b_1 n_g J_g J_r^2 - n_g J_g J_r a_{33}(K_r - a_{33}J_r) + a_{32}J_r^2 + n_g J_g(K_r^2 - a_{31}J_r) - b_2 n_g J_g J_r(K_r - a_{33}J_r)}{b_{32}n_g J_g J_r^2}$$

$$C_7 = -\frac{b_3 b_2 J_r J_g - b_{32}J_g(K_r - a_{33}J_r) - a_{32}J_r}{b_{32}J_g J_r}$$

$$C_8 = -\frac{J_r}{b_{32}} \quad (32)$$

TABLE I
CART WT CHARACTERISTICS

Rotor diameter	43.3 m
Transmission ratio	43.165
Tower height	36.6 m
Nominal power	650 kW
Maximum generator torque	$162/n_g$ kN.m

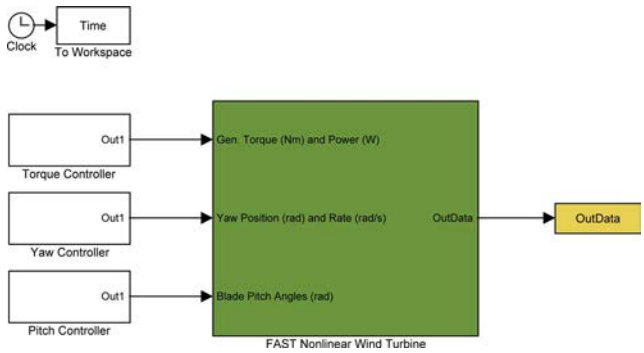

Fig. 5. FAST simulator block.

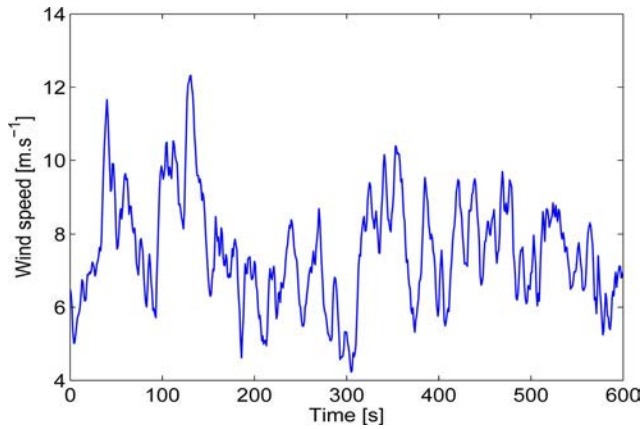

Fig. 6. Wind speed profile of 7 m/s mean value.

from the grid frequency. The supply side converter injects the generated power into the grid. Vector control techniques may be used in the ac side. A decoupled control of generator torque and flux is then possible. The main objective of the front-end converter control is to keep the dc-link voltage constant. More details are given on the back-to-back converter in [34] and [35]. The CART characteristics are given in Table I. A detailed description of this WT is given in [33].

CART was modeled with the mathematical model and the FAST aeroelastic simulator for validation (see Fig. 5).

The full-field turbulent wind set v used in this study is generated using SNWind developed by NREL. The hub-height wind speed profile is illustrated in Fig. 6. It consists of 600 s dataset of full-field turbulent wind that was generated using Class-A Kaimal turbulence spectra. It has a mean value of 7 m/s at the hub height and turbulence intensity of 25%.

In order to make a comparison between the proposed control strategies, all the simulations are carried out in the same conditions, as follows.

1) The presence of a constant additive control input disturbance d of $5/n_g$ kN ($n_g = 43.165$).

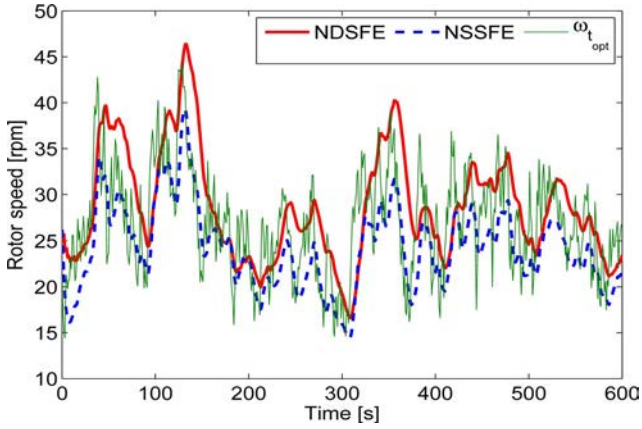

Fig. 7. Rotor speed using the two-mass mathematical model.

2) The presence of an additive measurement noise on ω_g with a SNR around 7 dB.
3) The same wind speed profile described earlier.

The parameters design for both controllers are presented in Appendix .

A. *Tests on the Simplified Mathematical Model*

The proposed controllers are first tested on the two-mass mathematical model. The parameters of the CART WT are given in Appendix C.

With the mathematical model, only the NSSFE and the NDSFE controllers performance are compared. In the next section, a global comparison of all the presented controllers, validated on FAST simulator, is performed. The rotor speed ω_t obtained using the two controllers on the mathematical model is shown in Fig. 7. Examining the optimal rotor speed $\omega_{t_{\rm opt}}$ profile, it can be seen that in order to achieve a compromise between energy capture improvement and dynamic loads reduction, an intermediate tracking dynamics should be chosen. The NDSFE controller shows a better performance when compared with the NSSFE. One can observe that the NDSFE controller ensures a rotor speed that tracks the mean tendency of the optimal rotor speed $\omega_{t_{\rm opt}}$, while avoiding the tracking of the short-time turbulence. The rotor turns more slowly with the NSSFE starting from the optimal rotor speed. This is visible along all the simulation. This deviation impacts the electrical power production of each controlled system. It is caused by the fact that the NSSFE controller is unable to reject the additive input disturbance. Concerning the control input, it can be observed from Fig. 8 that the generator torque $T_{\rm em}$ for both controllers is within the required constraint (under $162/n_g$ kNm). It remains smooth inducing low-frequency variations in the generator currents resulting in a less overheating of the generator and power electronics converter. The NSSFE control action is larger and excites a little bit more the drive train.

As depicted in Fig. 9, the electrical power P_e with the NSSEE controller is less important with the NDSFE one, especially when the wind speed exhibits fast variations as at instants 50 and 150 s.

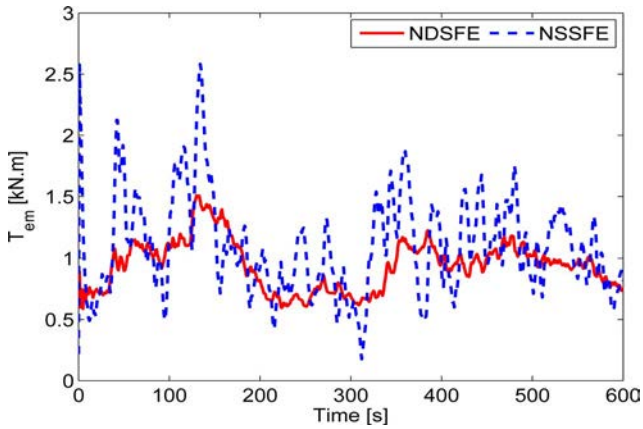

Fig. 8. Generator torque using the two-mass mathematical model.

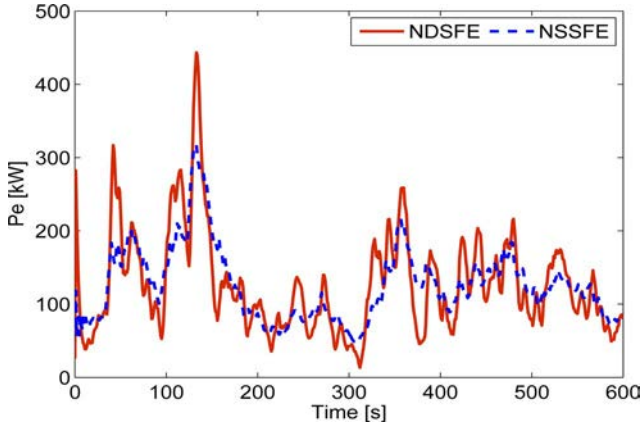

Fig. 9. Electrical power using the two-mass mathematical model.

B. Brief Simulator Description

The FAST code developed by NREL is an aeroelastic WT simulator that is capable of modeling two- and three-bladed propeller-type machines. This code is used by WT designers to predict both extreme and fatigue loads. It uses an assumed mode method to model flexible blades and tower components. Other components are modeled as rigid bodies. FAST uses an advanced certified code for modeling the aerodynamic behavior of the WT. It uses the blade element momentum (BEM) and a multicomponent wind speed profile for calculating WT loads [36]. It is a high fidelity aeroelastic simulator that was approved by Germanischer Lloyd (GL) WindEnergie GmbH for calculating onshore WT loads for design and certification [37]. For these reasons, FAST is adopted to validate the proposed nonlinear controllers with an estimator. In this study, 3 DOFs of the WT are considered: the variable generator and rotor speed (2 DOFs), and the blade teeter DOF. The variable generator and rotor speed DOFs account for the variations in generator speed and the drive-train flexibility associated with the torsional motion between the generator and hub/rotor. The blade teetering DOF accounts for the teeter motion induced by asymmetric wind loads across the rotor plane. FAST subroutines are coupled in an S-function to be incorporated in a Simulink model. Hence, FAST is interfaced with MATLAB Simulink (see Fig. 5).

TABLE II
SNWIND HUB-HEIGHT AERODYN FORMATTED WIND FILE COMPONENTS

Time
Horizontal wind speed
Wind direction
Vertical wind speed
Horizontal wind-shear, linear parameter
Vertical power-law, windshear exponent
Vertical wind-shear, linear parameter
Gust speed (not sheared by AeroDyn)

TABLE III
COMPARISON OF THE DIFFERENT CONTROL STRATEGIES BASED ON THE TWO-MASS MODEL USING FAST SIMULATOR

	MPPT	ATF	NSSFE	NDSFE
std(T_{ls})(kN.m)	11.37	11.76	10.91	9.23
max(T_{ls}) (kN.m)	78.69	89.33	68.32	54.65
std(T_{em})(kN.m)	0.274	0.279	0.266	0.244
max(T_{em})(kN.m)	1.80	1.98	1.61	1.52
$\eta_{\text{aero}}(\%)$	88.78	88.15	88.35	92.71
$\eta_{\text{elec}}(\%)$	68.75	69.34	71.97	74.953

FAST uses an AeroDyn file as an input for the aerodynamic part. AeroDyn is an element-level WT aerodynamics analysis routine. It requires information on the status of a WT from the dynamics analysis routine and returns the aerodynamic loads for each blade element to the dynamics routines [38]. AeroDyn has many options for the wind-input file. One option is simulated full-field wind data that represents all three components of the wind vector varying in space and time. Two files, one binary wind data file and one summary file, must be in the specific form generated by the NREL program SNLWind-3-D or SNWind. In this paper, input wind speed files are produced by SNWind [39]. SNWind includes parametrization files to specify the turbine/model specifications and the meteorological boundary conditions. SNWind can generate five different sets of output files. To be used with AeroDyn, it generates hub-height AeroDyn formatted files in a format compatible with AeroDyn. The format of the hub-height Aerodyn files used in this paper is given in Table II. It is AeroDyn routine that deduces the wind field around the turbine and computes the aerodynamic loads submitted by the WT. The hub-height horizontal wind speed is considered as the effective wind speed to be used with the two-mass mathematical model. However, with FAST, the WT undergoes a realistic wind field distribution. As mentioned in Table II, not only a single wind speed is used, but the wind direction, the vertical speed and the wind shear are taken into consideration.

C. Validation Using FAST Simulator

The developed controllers were implemented using the FAST flexible aeroturbine simulator interfaced with MATLAB Simulink. In order to make a comparison of the proposed methods, controllers performance are summarized in Table III.

One must keep in mind that the controllers objectives are power capture optimization while avoiding strong efforts on the drive-train and high-turbulent control torque. The controllers efficiency is compared using two criteria: the aerodynamic η_{aero}

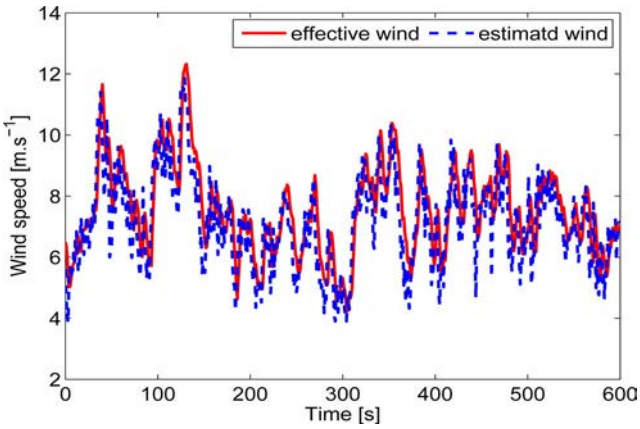

Fig. 10. Wind speed estimate.

and the electrical η_{elec} efficiency. They are defined as follows:

$$\eta_{\text{aero}}(\%) = \frac{\int_{t_{\text{ini}}}^{t_{\text{fin}}} P_a\, dt}{\int_{t_{\text{ini}}}^{t_{\text{fin}}} P_{a_{\text{opt}}}\, dt} \qquad \eta_{\text{elec}}(\%) = \frac{\int_{t_{\text{ini}}}^{t_{\text{fin}}} P_e\, dt}{\int_{t_{\text{ini}}}^{t_{\text{fin}}} P_{a_{\text{opt}}}\, dt} \tag{33}$$

where $P_{a_{\text{opt}}} = 1/2\rho\pi R^2 C_{p_{\text{opt}}} v^3$ is the optimal aerodynamic power corresponding to the wind speed profile and P_e is the electrical power. The low-speed shaft torsion and control torque minimization are measured by their variance and maximum.

All the controllers are evaluated with regards to different objectives.

1) Power capture optimization evaluated by the aerodynamic η_{aero} and the electrical η_{elec} efficiency defined in (33).
2) The control torque reduction and smoothing evaluated, respectively, by its maximum and standard deviation.
3) The transient loads reduction in the drive-train shaft evaluated by the low-speed shaft T_{ls} maximum and standard deviation.

All these values are given in Table III for all the controllers. The performance are also compared on the basis of different curves characterizing the controlled WT behavior. It is shown in [40] that these criteria are well adapted to evaluate the controllers.

As seen in Fig. 10, the estimator block used with the NDSFE provides a good estimate of the wind speed through the Kalman filter used with the Newton algorithm, despite the presence of measurement noise. The estimator then gives a correct reference speed $\hat{\omega}_{t_{\text{opt}}}$, thus enabling a better consideration of the dynamic aspect of the wind.

The rotor speed with the whole controllers and optimal rotor speed are depicted in Fig. 11. The effect of the input disturbance is clearly visible in the initial instants for the NSSFE. This effect also remains with the other controllers, except the NDSFE one, causing the rotor speed to deviate from its optimal tendency, especially for high-wind speed variations as at instants 50, 150, and between 300 and 400 s. All the controllers except the NDSFE are unable to reject the input disturbance. It can also be observed from Fig. 11 that the MPPT and ATF

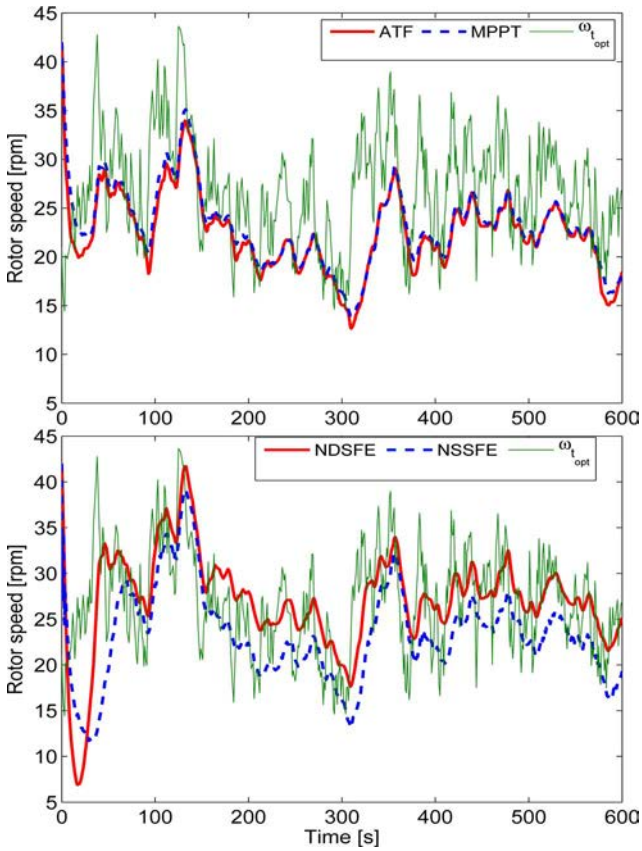

Fig. 11. Rotor speed ω_t with FAST simulator.

controllers react more slowly to the dynamic variations of the wind speed, compared to the NDSFE controller. The rotor speed with this controller tracks more closely the optimal rotor speed $\omega_{t_{\text{opt}}}$ leading to more power capture. The rotor speed with the NDSFE controller has a mean value of 27 r/min with a standard deviation of 5.26 r/min. After the start-up operation, the rotor speed deviation around its mean value is about 53 %. According to [5], this range of variation can be achieved by a WT equipped with a DFIG generator. In fact, the generator is not connected directly to the bus, but instead is coupled through the back-to-back converter inserted between the grid and the generator [29]. It allows the rotor to operate at a variable speed. Energy is then supplied to the grid at its frequency through the voltage-source converter.

For a better visibility of the control action constraint, the torque curves T_{em} and the low-speed shaft T_{ls} are gathered, for both controllers, in the same graphics (see Figs. 12 and 13). In terms of control loads presented in Fig. 12, referring to Table III, the maximal T_{em} value is around 2 kN with the ATF controller. Even though, it ensures the best power capture performance, the NDSFE needs the lowest maximum T_{em} value, compared to all the other controllers, with 1.5 kNm. Similarly with the T_{em} standard deviation, i.e., the lowest with the NDSFE and the highest with the ATF controller.

The fatigue loads on the drive train are represented by the low-speed shaft T_{ls} in Fig. 13. With the ATF controller followed by the MPPT, this value reaches its maximum, about 90 kNm.

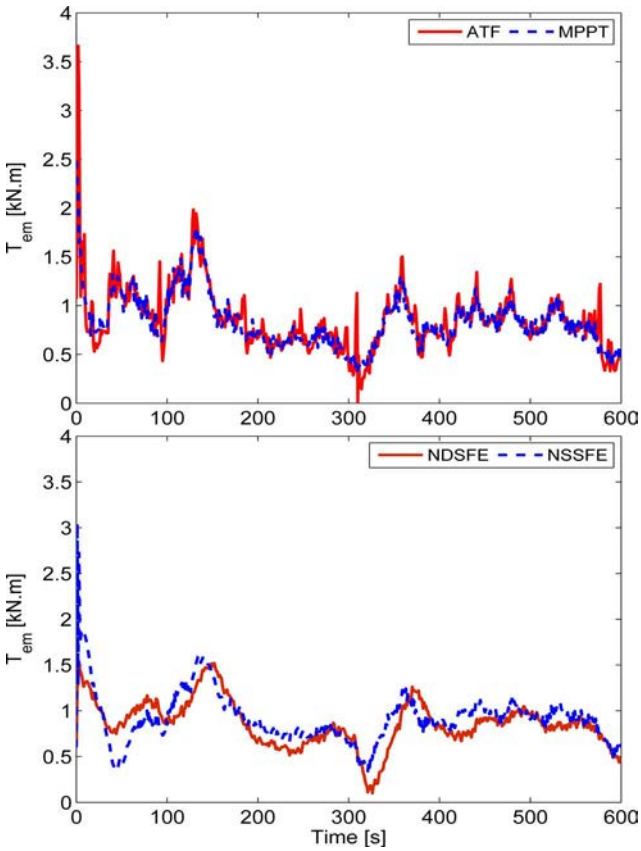

Fig. 12. Control torque $T_{\rm em}$ with FAST simulator.

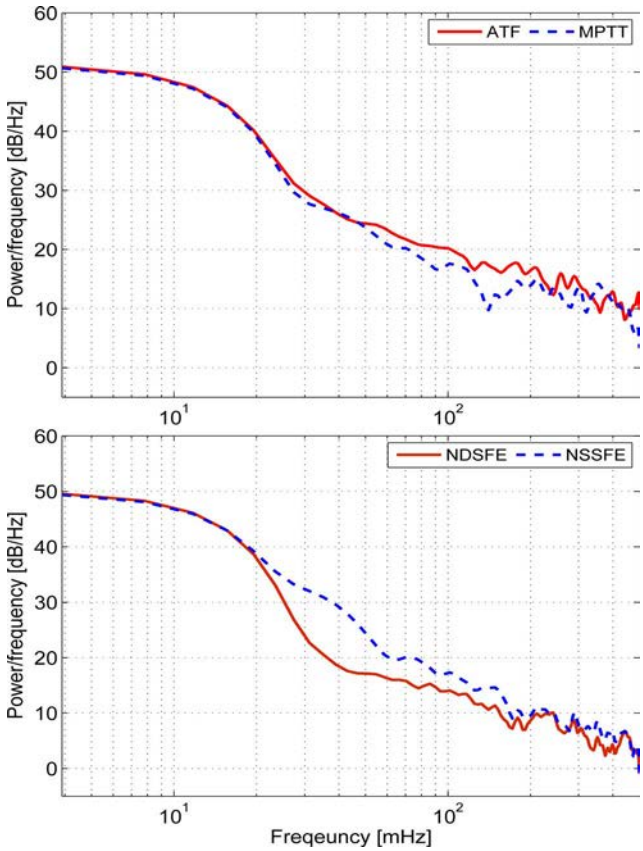

Fig. 14. Low-speed shaft torque PSD using FAST simulator.

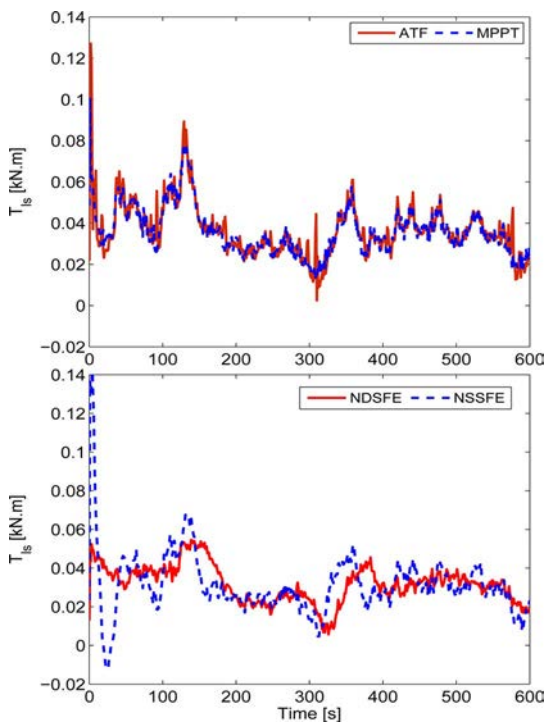

Fig. 13. Low-speed shaft $T_{\rm ls}$ with FAST simulator.

The lowest value of these maxima corresponds to the NDSFE with less than 55 kNm. Even though this last one ensures the best performance in terms of efficiency, the low-speed shaft remains equal to its lowest bound value (see Fig. 13).

The standard deviation of the low-speed shaft $T_{\rm ls}$ is also minimum for the NDSFE, as for the control loads $T_{\rm em}$. The MPPT and ATF transmit more torque to the generator. As explained in Section V-B, the MPPT and ATF controllers performances are imposed by the turbine characteristics. No DOF is available to tune these controllers. Therefore, their performance are limited in both power capture and control and transient loads. The good performance of the NDSFE controller can be explained by the smoothness of the control action, the success of the controller to reject the perturbation on the control torque and the consideration of the dynamic aspect of the wind.

In order to make a frequency analysis of the drive-train torque, the power spectral density (PSD) of the low-speed shaft $T_{\rm ls}$ is presented in Fig. 14 for all the controllers. It is also clear that it is the NDSFE controller, which minimizes the excitation of the drive train. Torsional resonance modes excitation is avoided by choosing a tracking dynamic that achieves a good compromise between power capture optimization by tracking the optimal tip–speed ratio and keeping a smooth control and transient loads on the low-speed shaft. A very fast tracking dynamic will induce a better power capture performance, but will produce a high turbulent control action. Conversely, a slow tracking dynamic will produce a smoother generator torque and rotor low-speed

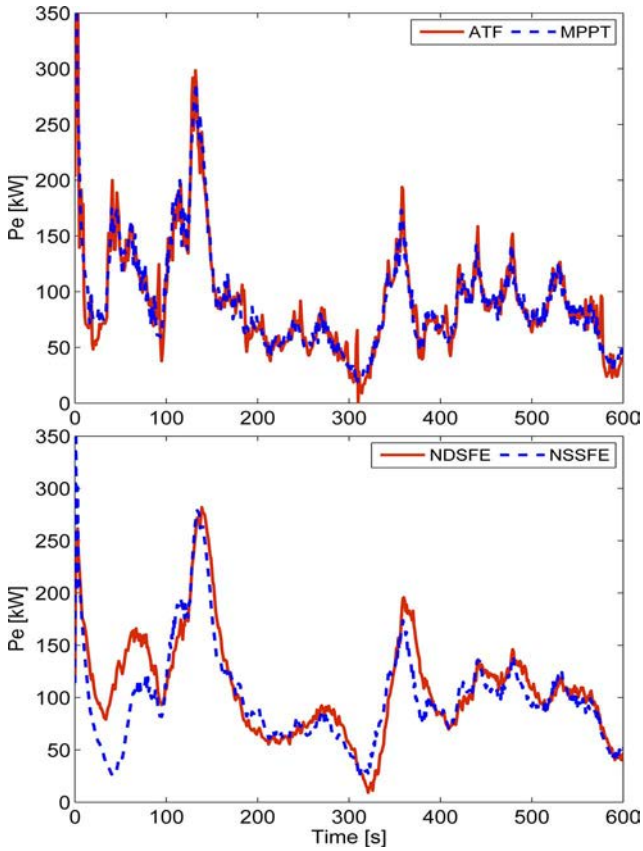

Fig. 15. Electrical power P_e with FAST simulator.

TABLE IV
NDSFE PERFORMANCE FOR DIFFERENT WIND SPEED PROFILES

Mean wind speed	Efficiency [%]	T_{hs} standard deviation [kN.m]	max T_{em} [kN.m]
7 m/s	74.95	9.23	1.52
8 m/s	76.22	14.03	1.60
8.5 m/s	73.50	12.55	1.86

shaft torque with less power capture efficiency. Therefore, an intermediate value is chosen for ensuring a time response of about 20 s for the tracking dynamics to achieve a compromise.

The better optimal rotor speed tracking leads to a more efficient electrical power production for the NDSFE controller, as shown in Fig. 15. According to the electrical power curves, the power produced by the WT using the nonlinear dynamic state feedback with a wind speed estimator (NDSFE), clearly shows better performance. The reason is that other control strategies are unable to reject the input disturbance. Besides, when the wind speed undergoes high variations, it is the NDSFE that best meets this solicitation and produces more energy. From Table III, one can note that the gap between the aerodynamic efficiency of the MPPT and the NDSFE controllers is, respectively, about 4% and 6% for the aerodynamic and electrical efficiency. This shows that the NDSFE technique takes in a better way into account the dynamic aspect of the wind due to the use of its estimate. The simulations are performed again with different wind speed profiles with other mean values below the rated one. The results are given in Table IV, which show that the NDSFE controller achieves similar performance even that the mean wind speed changes. As expected, the maximum electromagnetic torque increases with the mean wind speed value, nevertheless the standard deviation of the drive-train torque is smaller.

VII. CONCLUSION

In the aim of maximizing wind power capture for a two-mass WT model, classical ATF and MPPT control methods were adapted for this model. Nevertheless, they show a weak performance, particulary in the presence of input disturbance and measurement noise. Nonlinear static and dynamic state feedback controllers combined with an estimator, are then proposed, based on the two-mass model. The developed estimator allows the estimation of the aerodynamic torque as well as the effective wind speed and also all the state variables under consideration, from noisy measurements. As a result, it may be pointed out that the proposed nonlinear dynamic state feedback controller ensures better performance, in terms of efficiency with acceptable transient efforts on the low-speed shaft and control torque. Considering the dynamic aspect of the WT, its nonlinear aerodynamic behavior and the turbulent nature of the wind, jointly with the use of an estimator on the one hand and the perturbation rejection on the other hand lead to meet the aimed objectives.

APPENDIX A
WIND SPEED ESTIMATION ALGORITHM

For an instant t, the effective wind speed $\hat{v}(t)$ is obtained using Newton algorithm from the aerodynamic torque estimate $\hat{T}_a(t)$ and the rotor speed estimate $\hat{\omega}_t(t)$ given by the Kalman filter, as described in Section IV.

The iterative form of the algorithm is given as following.

Algorithm 1 Calculate $v = \hat{v}(t)$

Require: $N > 0$, $\varepsilon_{min} > 0$, $\hat{T}_a(t)$,$\hat{\omega}_t(t)$ and $\hat{v}(t - T_s)$
Ensure: $v = \hat{v}(t)$
1: $v \Leftarrow \hat{v}(t - T_s)$
2: $n \Leftarrow 0$
3: **repeat**
4: $\lambda_n = \dfrac{\hat{\omega}_t(t)R}{v}$
5: $H_n \Leftarrow -\rho\pi R^3 C_q(\lambda_n)v + \dfrac{1}{2}\rho\pi R^4 \hat{\omega}_t(t)\dfrac{\partial C_q(\lambda)}{\partial\lambda}$
6: $g_n \Leftarrow \hat{T}_a(t) - \dfrac{1}{2}\rho\pi R^3 C_q(\lambda_n)v_n^2$
7: $v_{old} \Leftarrow v$
8: $v \Leftarrow v - H_n^{-1} \cdot g_n$
9: $n \Leftarrow n + 1$
10: **until** $(n \geq N)$ or $(\frac{v - v_{old}}{v} \leq \varepsilon_{min})$
11: **return** v

APPENDIX B

CONTROLLERS PARAMETERS DESIGN

The optimal tip speed ratio $\lambda_{\rm opt}$ of the CART WT is equal to 8.5, corresponding to an optimal power coefficient $C_{p_{\rm opt}} = 0.4291$. Using the relationship

$$k_{\rm opt} = \frac{1}{2}\rho\pi\frac{R^5}{\lambda_{\rm opt}^3}C_{p_{\rm opt}}$$

the $k_{\rm opt}$ coefficient is then equal to 5.3813×10^3. The $k_{\rm opt_{hs}}$ coefficient of the MPPT controller is then deduced using (17) and is equal to 0.0669. The ATF controller tuning parameter is set to be $K_c = 3 \times 10^4$. The coefficients b_i are found by identification of the corresponding Hurwitz polynomial to a standard-order polynomial involving the damping coefficient and the crossover frequency, namely

$$s^2 + b_1 s + b_0 = s^2 + 2\xi\omega_0 s + \omega_0^2$$

leading to

$$b_0 = \omega_0^2$$
$$b_1 = 2\xi\omega_0$$

as $\omega_0 \approx 3/\xi t_r$, where t_r is the 5% setting time and ξ is the damping coefficient. By fixing ξ to 0.9, in order to achieve a time response t_r of 20 s, the constants b_0 and b_1 of the NSSFE characteristic polynomial are 0.0278 and 0.3000, respectively. For the third-order tracking dynamics, by expanding the characteristic polynomial

$$\frac{1}{10}(5\mathrm{s}+1)\cdot(2\mathrm{s}+1)\cdot(\mathrm{s}+1)$$

with a dominant pole at $s = -0.2$. In a similar manner, by identification through a third-order Hurwitz polynomial, one may get the coefficients b_i

$$\overset{(3)}{\varepsilon}_{\omega} + b_2\ddot{\varepsilon}_{\omega} + b_1\dot{\varepsilon}_{\omega} + b_0\varepsilon\omega = 0$$

where the constants b_0, b_1, and b_2 of the NDSFE are 0.1, 0.8, and 1.7, respectively.

APPENDIX C

TWO-MASS MODEL PARAMETERS

Rotor radius	$R = 21.65$ m
Air density	$\rho = 1.29$ kg/m^3
Rotor inertia	$J_r = 3.25 \cdot 10^5$ kg.m^2
Generator inertia	$J_g = 34.4$ kg.m^2
Shaft damping coeficient	$K_{ls} = 9500$ N.m/rad/s
Shaft stiffness coeficient	$B_{ls} = 2.691 \cdot 10^5$ N.m/rad
Rotor friction coefficient	$K_r = 27.36$ N.m/rad/s
Generator friction coefficient	$K_g = 0.2$ N.m/rad/s
Gearbox ratio	$n_g = 43.165$

REFERENCES

[1] J. F. Manwell, J. McGowan, and A. Rogers, *Wind Energy Explained: Theory, Design and Applications*. Hoboken, NJ: Wiley, 2002.

[2] P. W. Carlin, A. S. Laxson, and E. B. Muljadi, "The history and state of the art of variable-speed wind turbine technology," *Wind Energy*, vol. 6, pp. 129–159, Apr. 2003.

[3] J. Ernst and W. Leonhard, "Optimisation of wind energy output of variable speed wind turbines," in *Proc. Wind Power 85*, vol. 1, pp. 183–188, 1985.

[4] F. D. Bianchi, H. D. Battista, and R. J. Mantz, *Wind Turbine Control Systems: Principles, Modelling and Gain Scheduling Design*. Springer, 2nd ed., 2006.

[5] T. Burton, D. Sharpe, N. Jenkins, and E. Bossanyi, *Wind Energy Handbook*. Hoboken, NJ: Wiley, 2001.

[6] A. Mullane, G. Lightbody, R. Yacamini, and S. Grimes, "Adaptive control of variable speed wind turbines," in *36th Universities Power Eng. Conf.*, Swansea, U.K., 12–24Sep. 2001.

[7] L. Yazhou, A. Mullane, G. Ightbody, and R. Yacamini, "Modeling of the wind turbine with a doubly fed induction generator for grid integration studies," *IEEE Trans. Energy Convers.*, vol. 21, no. 1, pp. 257–264, Mar. 2006.

[8] Y. D. Song, B. Dhinakaran, and X. Y. Bao, "Variable speed control of wind turbines using nonlinear and adaptive algorithms," *J. Wind Eng. Ind. Aerodynam.*, vol. 85, pp. 293–308, Apr. 2000.

[9] H. Vihriälä, "Control of variable speed wind turbines," Ph.D. thesis, Tampere Univ. Technol., Tampere, Finland, Nov. 2002.

[10] F. Valenciaga and P. F. Puleston, "High-order sliding control for a wind energy conversion system based on a permanent magnet synchronous generator," *IEEE Trans. Energy Convers.*, vol. 23, no. 3, pp. 860–867, Sep. 2008.

[11] P. M. M. Bongers, "Modeling and identification of flexible wind turbines and a factorizational approach to robust control," Ph.D. thesis, Delft Univ. Technol., Delft, The Netherlands, Jun. 1994.

[12] T. Ekelund, "Modeling and linear quadratic optimal control of wind turbines," Ph.D. thesis, Chalmers Univ. Technol., Sweden, Apr. 1997.

[13] X. Ma, "Adaptive extremum control and wind turbine control," Ph.D. thesis, Denmark, May 1997.

[14] B. Beltran, T. Ahmed-Ali, and M. Benbouzid, "Sliding mode control of variable-speed wind energy conversion systems," *IEEE Trans. Energy Convers.*, vol. 23, no. 2, pp. 551–558, Jun. 2008.

[15] I. Munteanu, S. Bacha, A. Bratcu, J. Guiraud, and D. Roye, "Energy-reliability optimization of wind energy conversion systems by sliding mode control," *IEEE Trans. Energy Convers.*, vol. 23, no. 3, pp. 975–985, Sep. 2008.

[16] V. Galdi, A. Piccolo, and P. Siano, "Designing an adaptive fuzzy controller for maximum wind energy extraction," *IEEE Trans. Energy Convers.*, vol. 23, no. 2, pp. 559–569, Jun. 2008.

[17] C. Woei-Luen and H. Yuan-Yih, "Controller design for an induction generator driven by a variable-speed wind turbine," *IEEE Trans. Energy Convers.*, vol. 21, no. 3, pp. 625–635, Jun. 2006.

[18] S. A. Frost, M. J. Balas, and A. D. Wright, "Direct adaptive control of a utility-scale wind turbine for speed regulation," *Int. J. RobustNonlinear Control*, vol. 19, no. 1, pp. 59–71, 2008.

[19] W. E. Leithead and B. Connor, "Control of variable speed wind turbines: Design task," *Int. J. Control*, vol. 73, no. 13, pp. 1189–1212, 2000.

[20] H. Vihriälä, R. Perälä, P. Mäkilä, and L. Söderlund, "A gearless wind power drive: Part 2: Performance of control system," in *Eur. Wind Energy Conf.*, vol. 1, 2001, pp. 1090–1093.

[21] G. S. Stavrakakis and G. N. Kariniotakis, "A general simulation algorithm for the accurate assessment of isolated diesel-wind turbines systems interaction," *IEEE Trans. Energy Convers.*, vol. 10, no. 3, pp. 577–583, Sep. 1995.

[22] W. E. Leithead and M. C. M. Rogers, "Drive-train characteristics of constant speed HAWT's: Part I—Representatin by simple dynamic models," *Wind Eng.*, vol. 20, no. 3, pp. 149–174, 1996.

[23] W. E. Leithead and M. C. M. Rogers, "Drive-train characteristics of constant speed HAWT's: Part II—Simple characterisation of dynamics," *Wind Eng.*, vol. 20, no. 3, pp. 175–201, 1996.

[24] S. Muyeen, M. Ali, R. Takahashi, T. Murata, J. Tamura, Y. Tomaki, A. Sakahara, and E. Sasano, "Comparative study on transient stability analysis of wind turbine generator system using different drive train models," *IET Renew. Power Generat.*, vol. 1, pp. 131–141, Jun. 2007.

[25] R. Melício, V. M. F. Mendes, and J. P. S. Catalão, "Harmonic assessment of variable-speed wind turbines considering a converter control malfunction," *IET Renew. Power Generat.*, vol. 4, pp. 139–152, Mar. 2010.

[26] G. Ramtharan, N. Jenkins, O. Anaya-Lara, and E. Bossanyi, "Influence of rotor structural dynamics representations on the electrical transient performance of FSIG and DFIG wind turbines," *Wind Energy*, vol. 10, pp. 293–301, Jul./Aug. 2007.

[27] B. Boukhezzar, H. Siguerdidjane, and M. Hand, "Nonlinear control of variable-speed wind turbines for generator torque limiting and power optimization," *ASME J. Solar Energy Eng.*, vol. 128, pp. 516–530, Nov. 2006.

[28] B. Boukhezzar, L. Lupu, H. Siguerdidjane, and M. Hand, "Multivariable control strategy for variable speed, variable pitch wind turbines," *Renew. Energy*, vol. 32, pp. 1273–1287, Jul. 2007.

[29] A. Mullane and M. O'Malley, "The inertial response of induction-machine-based wind turbines," *IEEE Trans. Energy Convers.*, vol. 20, no. 3, pp. 1496–1503, Aug. 2005.

[30] J. B. Ekanayake, L. Holdsworth, X. G. Wu, and N. Jenkins, "Dynamic modelling of doubly fed induction generators wind turbines," *IEEE Trans. Power Syst.*, vol. 18, no. 2, pp. 803–809, May 2003.

[31] B. Boukhezzar and M. M'Saad, "Robust sliding mode control of a DFIG variable speed wind turbine for power production optimization," in *Proc. 16th Mediterranean Conf. Control Automat.*, Jun., 2008, pp. 795–800.

[32] B. Boukhezzar and H. Siguerdidjane, "Nonlinear control with wind estimation of a DFIG variable speed wind turbine for power capture optimization," *Energy Convers. Manage.*, vol. 50, no. 4, pp. 885–892, 2009.

[33] L. J. Fingersh and K. Johnson, "Controls advanced research turbine (CART) commissioning and baseline data collection," NREL Report TP-500-32879, National Renewable Energy Laboratory, Golden, Co, Oct. 2002.

[34] R. Ottersten, "On control of back-to-back converters and sensorless induction machine drives," Ph.D. thesis, Chalmers Univ. Technol., Göteborg, Sweden, 2003.

[35] R. Pena, R. Cardenas, R. Blasco, G. Asher, and J. Clare, "A cage induction generator using back to back PWM converters for variable speed grid connected wind energy systems," in *Proc. IECON 2001*, pp. 1376–1381.

[36] M. Hansen, J. Sørensen, S. Voutsinas, and N. Sørensen, H. Madsen, "State of the art in wind turbine aerodynamics and aeroelasticity," *Prog. Aerospace Sci.*, vol. 42, no. 4, pp. 285–330, 2006.

[37] A. Manjock, "Design codes FAST and ADAMS® for load calculations of onshore wind turbines," Tech. Rep. No. 72042, Germanischer Lloyd WindEnergie GmbH, Hamburg, Germany, May 2005.

[38] D. J. Laino and A. C. Hansen, *User's Guide to the Wind Turbine Aerodynamics Computer Software Aerodyn*. National Wind Technology Center, National Renewable Energy Laboratory, Golden, Colorado, 12.50 ed., Jul. 2003.

[39] M. L. Buhl, *SNwind USER's GUIDE*. National Wind Technology Center, National Renewable Energy Laboratory, Golden, Colorado, 1.2 ed., Jun. 2003.

[40] A. Heege, Y. Radovcic, and J. Betran, "Fatigue load computation of wind turbine gearboxes by coupled structural, mechanism and aerodynamic analysis," *DEWI Mag.*, no. 21, pp. 61–68, 2006.